OpenNano 9 (2023) 100120

Contents lists available at ScienceDirect

OpenNano

journal homepage: www.elsevier.com/locate/onano

Full length article

Smart suture with iodine contrasting nanoparticles for computed tomography

Shadi Houshyar [a,*], Hong Yin [a], Leon Pope [a], Rumbidzai Zizhou [b], Chaitali Dekiwadia [c], Elisa L. Hill-Yardin [d], Justin MC Yeung [e], Sabu John [a], Kate Fox [a], Nhiem Tran [f], Ivan Cole [a], Aaron Elbourne [f], Vi Khanh Truong [f,g], Adam Truskewycz [h,*]

[a] School of Engineering, STEM college, RMIT University, Melbourne, Australia
[b] Center for Materials Innovation and Future Fashion (CMIFF), School of Fashion and Textiles, RMIT University, Australia
[c] RMIT Microscopy & Microanalysis Facility, College of Science, Engineering and Health, RMIT University, Melbourne, 3000, Australia
[d] School of Health & Biomedical Sciences, RMIT University, Bundoora, Australia
[e] Department of Surgery, Western Health, Western Precinct, University of Melbourne, Australia
[f] College of Science, STEM college, RMIT University, Melbourne, 3000, Australia
[g] College of Medicine and Public Health, Flinders University, Bedford Park, SA, Australia
[h] Department of Biomedicine, University of Bergen, Bergen, Norway

ARTICLE INFO

Keywords:
Contrast agent
Antimicrobial resistance
Surgical site infection
Suture
Core-shell filament

ABSTRACT

Surgical site infections (SSI) are amongst the most common medical infections, occurring in 2 to 4% of patients undergoing a surgical procedure. Smart surgical sutures can play an important role in preventing infection. For example, antimicrobial sutures detectable via clinical imaging modalities can support monitoring wounds post-surgery and enhance patient recovery. However, no commercial suture products possess these properties. Herein, contrasting iodine carbon nanoparticles (ICPs) are synthesized using a solvothermal approach. These ICPs were incorporated into polycaprolactone (PCL) via a coaxial extrusion technique inspired by the "core-shell" multilayered suture structure, which integrates multiple clinically favourable functions into one suture device. This system exhibits high imaging contrast capabilities for real-time imaging even after 22 days *in-vitro*, with strong antimicrobial properties and a reduction in biofilm formation. The multifunctional and biocompatible suture composite developed in this study shows strong antimicrobial properties and can act as an immobilized marker to monitor the surgical site during and after surgical procedures. Identifying suture integrity and location within the body through minimally invasive methods can alleviate patient discomfort and minimize the risk of infection.

1. Introduction

A suture is one of the most widely implanted material in the human body during surgical procedures. Generally, a suture is used for wound closure and to support the wound-healing process. It exists in degradable and non-degradable forms. The degradable suture provides temporary support to the wound until the wound heals well enough to withstand everyday stress, while the non-degradable

* Corresponding authors.
E-mail addresses: shadi.houshyar@rmit.edu.au (S. Houshyar), adam.trusk@gmx.com (A. Truskewycz).

https://doi.org/10.1016/j.onano.2022.100120
Received 9 June 2022; Received in revised form 29 November 2022; Accepted 13 December 2022
Available online 14 December 2022

sutures stay longer, provide more strength and support, and should be removed after serving their purpose. As mentioned in the literature and clinical studies, the sutured wound is susceptible to infection due to the applied stress and strengthening of the surrounding tissue around the wound [1–3]. Furthermore, the adhesion of bacteria onto the surface of the suture increases due to its suture structure and subsequent biofilm formation, which when it occurs, can cause infection. If the wound gets infected, it is notoriously resistant to treatment, even with high doses of antibiotics [4–7]. As mentioned in the literature, the bacteria usually multiply in the infected wound where necrosis is present or where blood is pooled into the wound, resulting in a red, hot, swollen, and painful wound. Also, it can result in wound opening and lead to wounding complications after surgery. If the infected wound is inside the body, it is difficult to detect wound opening and infection by the patient or clinician without surgical intervention. Therefore, a smart suture remotely monitored by imaging modalities can reduce the risk of infection and benefit the patient.

Commercial contrast agents, used for oral and intravenous contrast, including barium sulfate and iodine, are not used in the clinical practice of coating sutures due to inherent toxicities, short half-lives, and solubility materials in organ compartments [8]. Therefore, many researchers initiated research on materials with variable visibility in imaging [9–11]. For example, Shin et al. (2017) developed core-shell structured tantalum oxide-silica nanoparticles as a tissue adhesive in image-guided surgery; however, there were issues with poor biodegradability [12]. Another study reported a 3D-printed mesh with iodine and barium as the contrast agent. However, only it maintained visibility for seven days in the media [8].

Radiopaque materials have drawn attention worldwide for many years as they have diverse applications in the medical field. The greater the radiopacity, the greater the contrast it creates with the neighbouring tissue enabling the clinician to identify and interpret the position of this foreign material for future surgical management. In a study on a flexible radiopaque suture by Sneha et al. [13], dip-coated sisal fibres with SrO-integrated PLA made them radiopaque with excellent tensile properties without compromising their flexibility [13]. This suture showed great antimicrobial properties during 28 days in media as the loaded ciprofloxacin released slowly over time. Furthermore, radiopaque iodine nanoparticles have been previously used as a contrasting agent in Computed Tomography (CT imaging, Fig. 2) [14]. Numerous studies have developed iodine composites for imaging and/or theragnostic applications [15–18]. For example, Nimmy et al. investigated crosslinking silk with an iodine compound to make suture visible in situ. These modified silk sutures demonstrated high tensile properties, no toxicity, good visibility and antimicrobial properties due to the slow release of linked

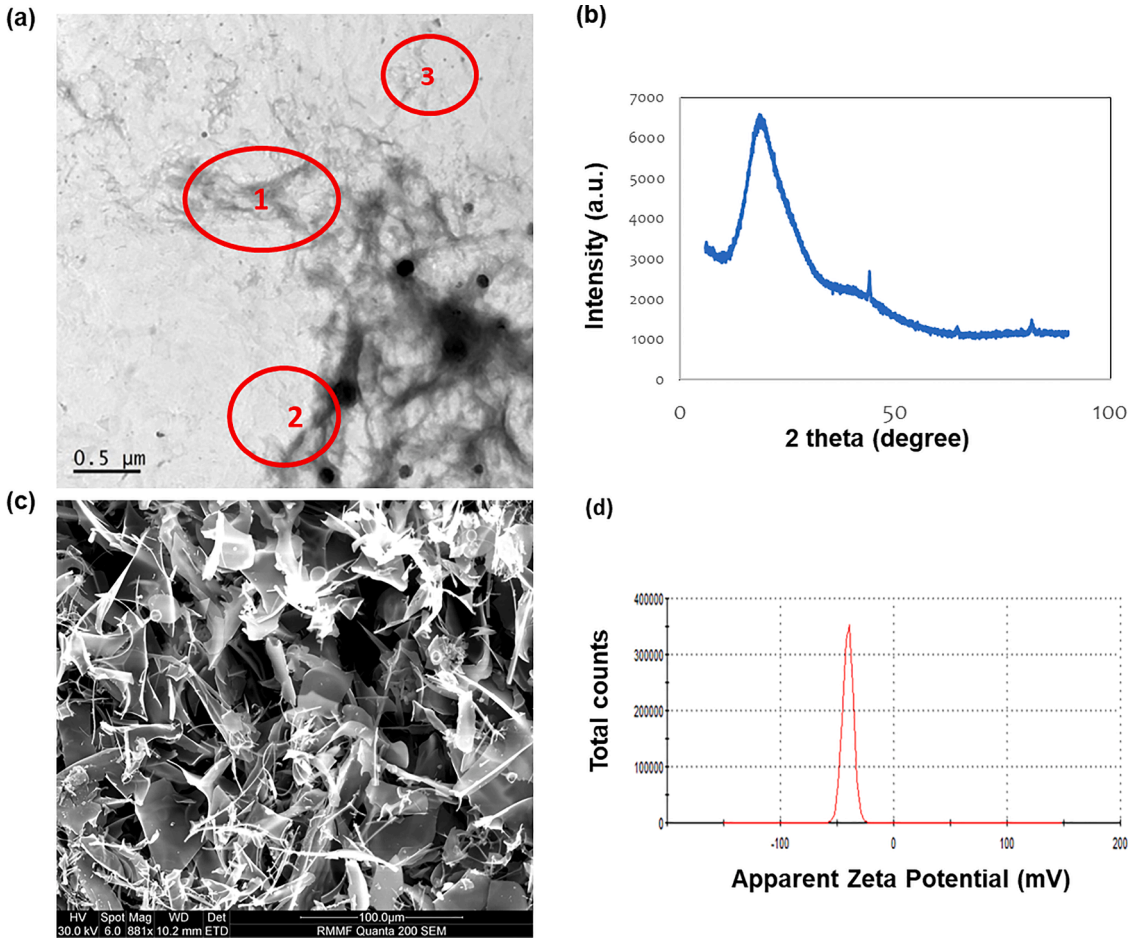

Fig. 1. (a) TEM images 1, 2 and 3 are particles in the image (b) XRD spectra (c) SEM and (d) Zeta potential of ICPs.

iodine to the surrounding tissue. Furthermore, Ikeda et al. investigated the iodine-containing calcium titanate for infection control of orthopaedic and dental implants and confirmed its safety in the physiological system [19]. Also, another study demonstrated that molecular iodine is not responsible for cytotoxicity in commercial contrast agents iodophors [20]. However, as mentioned above, currently, there is no commercial contrast material that can be used within suture products due to inherent toxicity properties. As a result, it is suggested that contrast materials should be linked chemically or physically to prevent quick release into the surrounding environment and, thus, prevent toxicity. This study highlighted a method of imparting radiopacity to Polycaprolactone as a suture material using iodine-conjugated carbon nanoparticles, Fig. 1S (Supporting Information), to lower the iodine toxicity and prolong the lifetime of the contrast agents. PCL fibres were composed of the iodine carbon dots core that provides radiopacity and extra strength to the PCL fibres as well as prevents or controls the release of iodine carbon particles (ICPs) to the environment. The core-shell PLA fibres were evaluated for radiopacity and were mechanically tested for suture applications. *In-vitro* degradation studies and cell viability were performed alongside antimicrobial testing.

2. Experimental section

Fabrication of ICP. Phloroglucinol (9 g), iodoacetic acid (3 g), and cysteine (3 g) were added to methanol (30 mL) and 2amino-2methyl-1propanol (AMP) (15 mL). After forming a transparent solution, the mixture was put into hydrothermal vessels at 195 °C for 7 h. The brown-yellow products were cooled to room temperature and transferred onto a dialysis membrane (molecular weight cut-off of 1000 Da). The product was dialyzed against ultrapure water for 7 d to remove unreacted residues. After dialysis, the product was subjected to a freeze dryer to obtain dry powders. [14] Then, the ICPs were embedded into PCL through wet spinning to make an I-PCL suture. I-PCL sutures with various amounts of ICP concentration, 0, 10, 20, 30 and 40% were identified as 0I-PCl, 10I-PCL, 20I-PCl, 30IPCLl, and 40I-PCL sutures, respectively, Table 1.

Analysing ICPs: Powder X-ray diffraction (XRD) patterns were collected on a Bruker AXS D8 Discover diffractometer equipped with a Cu Kα radiation source (λ = 1.5418 Å) operating at 40 kV and 35 mA. All X-ray data were obtained in the μ−2θ locked couple mode over a 2θ range of 5 − 90° Fourier transforms infrared (FTIR) spectra of materials were recorded by an FTIR spectrometer (PerkinElmer, Frontier) with an average of 32 scans per sample and a resolution of 16 cm^{-1} in the range of 4000−700 cm^{-1}. Surface charges (zeta potentials) were measured using a Malvern 885 2000 Zetasizer in DI water, Fig. 2.

Fabrication of I-PCL sutures; Poly (ε-caprolactone) (PCL) (Mw - 57,000–90,000 g/mol) was purchased from Sigma Aldrich, Australia. The wet spinning technique was used to fabricate ICP-embedded PCL filaments. The 20% PCL solution in DMF was prepared to be used for the shell structure, and various amounts of ICP (0, 10, 20, 30 and 40%) were added to the PCL-DMF solution to make a solution for the core suture. The wet spinning parameters, such as feeding rate, collector speed, and needle size, were optimized by preliminary experiments. The 20% PCL spinning dispersion with ICP (I-PCL) was placed in a syringe used for the fibers core component, and the component without ICP was placed in the syringe used for the shell structure, Fig. 1(a). For the shell and core, the spinning solutions were pumped into a coagulation water bath through a coaxial nozzle, with an 18 and 22-gauge spinneret, respectively. The feeding rates were 8 and 5 ml/hr for the shell and core, and the filament was collected on a tubular drum at 100 rpm, Fig 1(a). After spinning, the I-PCL filaments (sutures) were dried at room temperature for 3 days. The details of the prepared samples are described in Table 1.

Assessment of Antibacterial Properties: Bacterial strains used in this study were obtained from the American Type Culture Collection for MRSA (ATCC® 700699). Bacterial culture was grown in tryptic soy broth (TSB). Samples were incubated with 2 mL of bacterial culture with an optical density of 600 nm of 0.1. These samples in the bacterial culture were incubated at 37 °C for 18 h without shaking. Prior to the analysis, samples were washed twice with sterile PBS.

Confocal laser scanning microscopy (CLSM) was performed on a ZEISS LSM 880 Airyscan upright microscope. Bacterial cells were dyed using a LIVE/DEAD BacLight Bacterial Viability Kit (SYTO 9 and propidium iodide, Molecular Probes Invitrogen, Grand Island, NY, USA) with an incubation period of 15 min at 25 °C according to the manufacturer's protocol. The SYTO 9 dye binds to nucleic acids in viable and non-viable cells and fluoresces green when excited at 485 nm. Propidium iodide (P.I.) can only enter cells that are no longer viable once they have undergone significant membrane damage. In addition, P.I. has a higher binding affinity towards nucleic acids present in bacterial cells than the SYTO 9 dye. P.I. fluoresces red when excited by a 535 nm wavelength laser, representing dead cells. At least three areas of interest were examined, obtaining 3 × 3 imaging grids of 377 × 377 μm^2 confocal images for each sample investigated. The surface-cell population was homogenous in general. The number of live and dead cells was quantified using Cell-C software for all images obtained (https://sites.google.com/site/cellcsoftware/).

Cell viability assay: L929 mouse fibroblasts were used to test the *in-vitro* cytotoxicity of the I-PCL sutures (the filaments were approximately 250 μm in diameter). The cell culture medium was Dulbecco's modified Eagle's medium (DMEM) solution supplemented with 10% FBS and 1% penicillin/streptomycin. Prior to the cell viability assay, 5 mg of each I-PCL filament was weighed and adhered to the bottom of a 48-well cell culture plate using 0.1 g of clear 100% silicone glass sealant (Selleys). The well-plate was then covered and left to dry for 5 days at room temperature. After 5 days, samples were rinsed by micropipette 500 μL Milli-Q water into

Table 1
Details of developed I-PCL sutures used in this study.

Sample name	0I-PCL	10I-PCL	20I-PCL	30I-PCL	40I-PCL	40I
ICP concentration (%)	0	10	20	30	40	40
ICP core-PCL shell	√	√	√	√	√	Core only

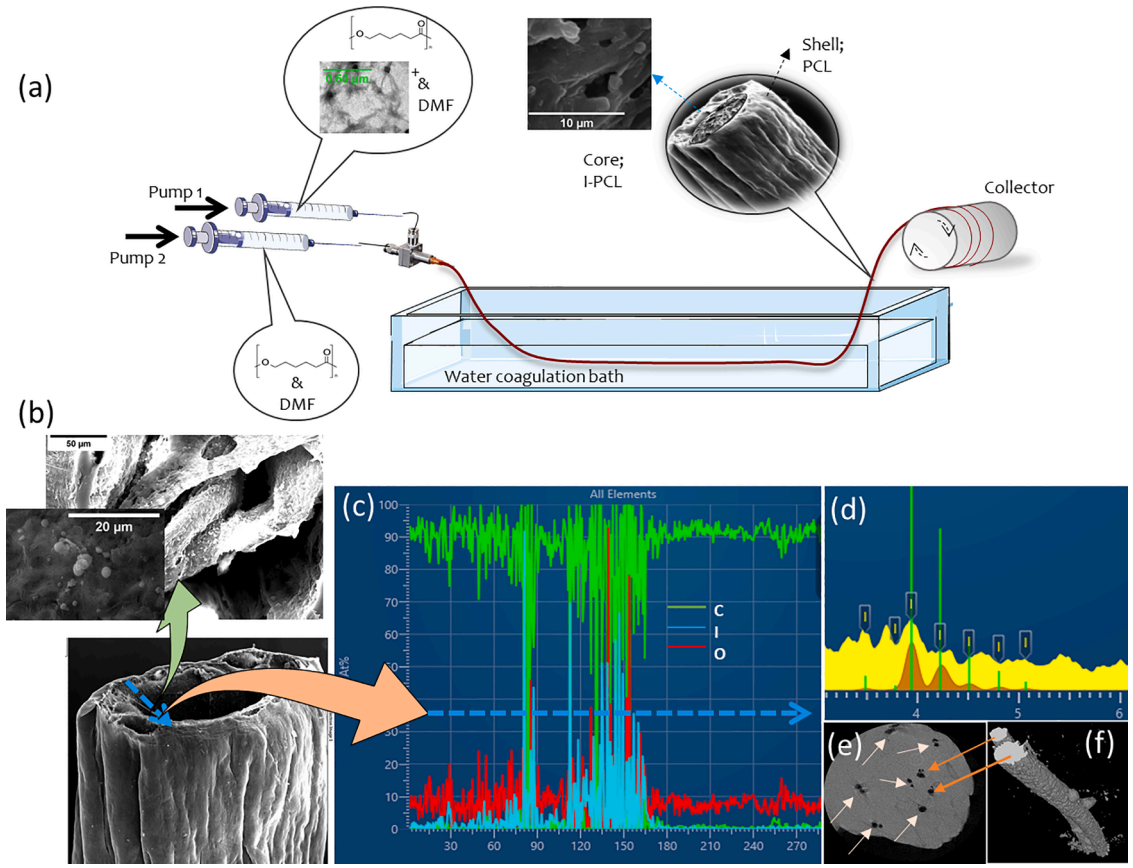

Fig. 2. Fabrication method, morphology, composition and radiopaque properties of the coaxial filament. (a) Schematic showing the method of embedding ICP into core-shell suture filaments; the polymer solution with (pump 1) and without ICP (pump 2) was placed in two syringes for the core and shell materials, and the solution in the syringes was pumped into the water coagulation bath through the coaxial nozzle and collected by the drum (b) SEM images of the core-shell structure of suture; the blue arrow shows the direction of Energy dispersive spectroscopy (EDS) scan (c, d) EDS of the fibre cross-section showing the presence of iodine in the middle part of the fibres (hollow parts) and not on the outer wall; the blue arrow, spectrum is from the hollow section (middle part) of the filament; (e) Micro-computed tomography (CT) images showing the cross-section of the chicken breast with core-shell filaments in it, light orange arrows indicate the presence of suture in the cross-section of the chicken breast (f) the filaments constructed from CT scan image of image e.

each well, removing the water, and lightly dabbing each well with Kim wipes (Kimtech Science). Before seeding the cells, the 48 well plates were sterilized via U.V. sterilization (ProCleaner Plus, BioForce Nanosciences). L929 cells were seeded at a concentration of 10,000 cells in 400 µL cell culture media and were incubated at 37 °C, 5% CO_2 for 48 h. Cells grown directly on the silicone adhesive without I-PCL sutures were used as a control. Next, L929 cell viability was quantified using a resazurin assay. For this, 40 µL of alamarBlue Cell Viability Reagent (Invitrogen) was pipetted into each well. The plates were incubated at 37 °C for 4 h, and then the fluorescence was analysed using a microplate reader (Spectramax Paradigm) excitation peak at 560 nm and an emission peak at 590 nm. The fluorescence was normalized to that measured from the control cells grown on the silicone adhesive.

Each sample was rinsed with PBS and fixed with 4% formalin in PBS for 10 min to image the cells via confocal microscopy. Samples were then rinsed twice with PBS to remove excess formalin and permeabilized with 1% Triton X-100/PBS for 3 min. After permeabilization, the samples were rinsed twice with PBS, blocked with 1% bovine serum albumin for 15 min and rinsed twice with PBS. Rhodamine Phalloidin and DAPI (ThermoFisher) were then used to stain actin filaments and nuclei, respectively. Samples were washed twice with PBS and then stored in 600 µl PBS at 4 °C for CLSM. To prepare the samples for CLSM, the filaments were extracted from the well plates using fine-tipped tweezers, inverted at 180° and placed on a 35 mm glass-bottom dish. Next, 200 µl PBS was pipetted on top of the filaments, and a glass coverslip was placed. CLSM images were taken using the Nikon A1/Ti-E confocal microscope.

I-PCL suture analysis: Microstructure and elemental analyses were performed using FEI Verios 460L XHR-SEM equipped with Energy-dispersive X-ray spectroscopy (EDS) @10 kV on 10 nm iridium-coated filament. The contrast properties were recorded using a Bruker Skyscan 1275 Micro CT, @30 kV with no filter, 360° and 2 frames per second scanning rate. Attenuated Total Reflectance Fourier Transform Infrared (ATR-FTIR) spectroscopy was used to identify the types of chemical bonds and functional groups in the composite fibres. The FTIR spectra were collected using a PerkinElmer Spectrum-400 spectrometer with 64 scans per spectrum. *X-ray photoelectron spectroscopy (XPS)* was undertaken using a Thermo-Fisher K-Alpha with an Al Kα source. The samples were scanned using

a spot size of 400 μm, power of 300 W and the application of the flood gun to remove any sample charging. The XPS scanned the top 2–5 nm of the sample surface. Survey spectra were attained using a pass energy of 200 eV with a step size of 1 eV and dwell time of 50 ms, whilst the high-resolution spectra of C1s and I3d were assessed with a pass energy of 50 eV and a step size of 0.1 eV.

X-ray computed tomography of breast and thigh tissue: Fresh chicken breast and thigh were used, inserting 40I-PCL into the chicken breast and thigh using sewing needles. Prepared samples were imaged with a Bruker Skyscan 1275 Micro-C.T. using the previously mentioned imaging parameters. The slices were post-processed into 3D reconstructions using cone-beam reconstruction software (Skyscan NRecon. The image analysis and segmentation processes include filter, and adaptive thresholds with the CTAn and CTVol software for quantitative and visualization purposes.

Degradation study of I-PCL sutures in PBS: The release of ICP to the media was investigated by immersing the sutures into a vial containing 5 mL PBS (pH 7.3) at 37 °C with 100 rpm shaking. Then, at different time intervals for 22 days, aliquots were taken for further analysis and the vial was refilled with the same volume of fresh PBS. The collected liquid was analysed under a UV–Visible-NIR detector (Agilent Carry 5000) from 200 nm to 800 nm for determination of ICP concentration in the accumulated liquid was performed using an Agilent HP 7700 series Inductively Coupled Plasma Mass Spectrometer (ICP-MS). ICP standard solution was prepared from 99.99% potassium iodide (Chem Supply Australia) in the concentration range of 0 to 100 μg/L. Following the method mentioned above, the collected I-PCL sutures collected at 22 days were analysed under FTIR, EDX, SEM, and XPS. The experiments were performed in triplicate, and the results were reported as an average of three.

Statistical analysis: The results were reported as an average, and the appropriate standard deviations were calculated. A One-way ANOVA was used to analyse the statistical significance between the means of different samples using M.S. Excel.

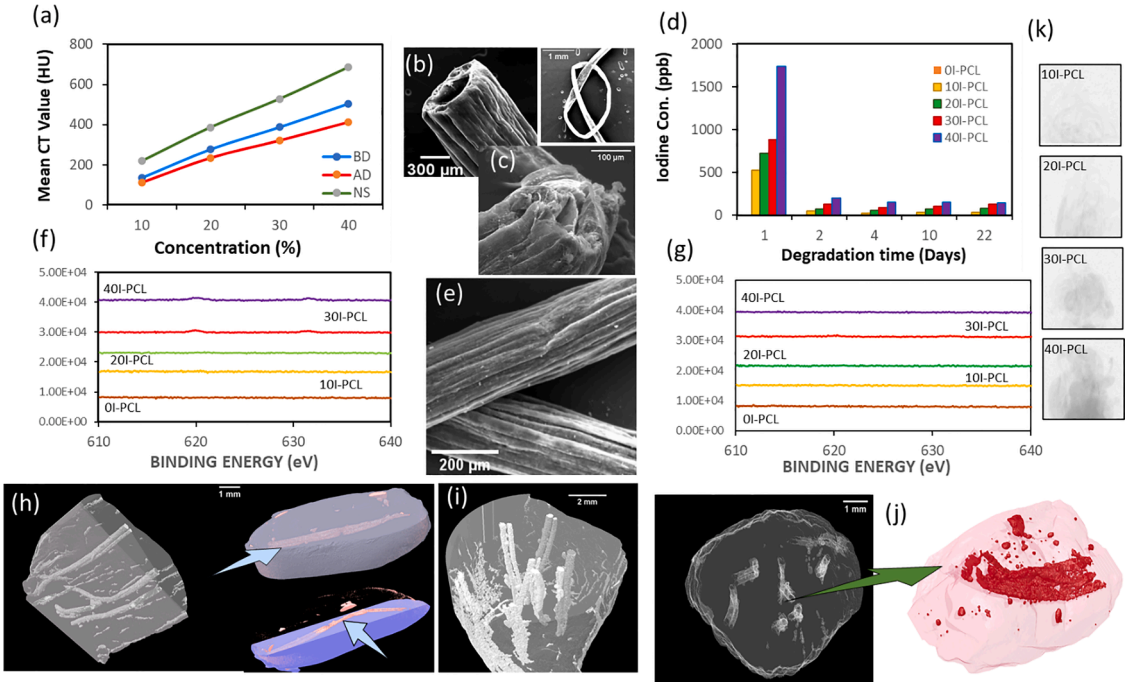

Fig. 3. Radiopacity and morphological properties of the coaxial filament before and after degradation. (a) The highest attenuation (mean HU) vs ICPs concentrations show a linear increase of HU with ICP concentration with no significant drop in HU for the degraded samples (AD) after 22 days in PBS in comparison with the virgin sample (BD), the highest HU belongs to the suture with core only and no shell (NS) (b) SEM images of sutures and the possibility of making knots without breaking the fibres. (c) the cross-section after the mechanical test (d) The release of ICP was recorded over 22 days in the PBS. The burst release is in the first 24 hrs, followed by slow release till day 22, which shows the controlled release of ICPs to provide antimicrobial properties while providing enough contrast properties to be visible under the C.T. scan (e) SEM of the ICP filament surface, showing the wrinkled surface as expected. (f) and (g) XPS spectra of the suture with various ICPs concentrations before and after degradation. As measured, the ICP on the surface of the filament, the intensity of the peak is too small, and they are mainly deposited during the fabrications. After degradation, there is no ICP on the filament surface due to the release of ICPs deposited during the fabrication to the media. (h), (i) and (j) rendered images of the suture in the chicken tissue, with a blue arrow pointing to the single filament in the chicken breast. Based on the microCT scan results, the presence of the suture is clear and visible inside the chicken tissue (red dots indicate the broken segments of the suture) (j) cross-section of the chicken breast with the suture inside (k) MicroCT images of the PCL filament with various ICP core concentration.

3. Results and discussion

3.1. Synthesis and characterization of iodine contrasting nanoparticles (ICPs)

The generated ICP compound possesses a brown colour with porous morphology, Fig 1 (a & c). It is sparingly soluble in water but can easily dissolve in ethanol and other organic solvents. Furthermore, its surface is negatively charged as measured in DI water with a zeta potential of −40 mV, suggesting the presence of abundant functional groups such as COOH. These groups can support attaching to other materials to provide surface modification, Fig. 2S(d) (Supporting Information). The possible structure of the ICP compound is presented in detail in Fig. 1S(b) (Supporting Information).

In the XRD diffractogram of ICPs, the broad peak at $2\theta = 19.3^{\circ}$ indicates an amorphous carbon structure (Fig 1(b)). This peak position corresponds to the (002) hkl plane of carbon interlayer spacing ($d = 0.46$ nm). Similar to the reported carbon dot material disordered stacking of CQDs with sp [2] carbon structures, the spacing is higher than the graphitic interlayer (0.33 nm). That should be attributed to the polymer network. In addition, there are some small but sharp peaks at higher diffraction angles; they may correspond to the crystalline graphite structure (100) produced in the hydrothermal process. From the TEM image, Fig. 1(a) and based on the chemistry of precursors, there are three possible components in the synthesized carbon materials, shown in Fig. 1S (Supporting Information).

The chemical composition of the ICP compound is determined by FTIR (Fig 12S(a), Supporting Information). A broad absorption band at about 3300 cm^{-1} is associated with the stretching vibration of N—H and O—H. The peaks at 1600 and 1705 cm^{-1} indicate the presence of C = C stretching and carbonyl (C = O) groups, C–H stretching vibrations at 2940 cm^{-1}, C = C stretching vibrations at 1660 cm^{-1}, C–N stretching vibrations at 1410 cm^{-1}, and C–H stretching vibrations at 1070 cm^{-1}. Additionally, the absorption peak at 438 and 549 cm^{-1} are related to the vibration of I–O, which proves the incorporation of iodine during synthesis [8,17].The peak at 1600 cm^{-1} is related to the C = C stretching of sp [2] hybridization.

Characterisation of ICP embedded-Polycaprolactone (I-PCL) filament. As shown in Fig. 2, the wet spinning technique was used in this study to fabricate the filament with enhanced contrast properties. The scanning electron microscopy (SEM) images of the filament (Fig. 3(b)) confirmed the core-shell structure of the filament. The shell structure is wrinkled due to the partial collapse of the core during the drying process due to the high concentration of solvent in the core section of the filament. The shell partially collapses when the solvent evaporates from the middle section of the filament, as it cannot support the applied stress from the shell structure and causes mild wrinkling. Additionally, a faster injection speed of the shell solution than the core solution resulted in inadequate core materials to support the shell. Therefore, it led to a limited collapse and wrinkling of the shell structure.

The ICP-PCL filament composition was analysed with FTIR (Fig 2S, Supporting Information). Most of the peaks represent that the ICPs are hidden or overlapped with PCL peaks; however, a peak at 1601 cm^{-1} is clearly visible in most of the spectrum and is assigned to C=C stretching vibrations of sp [2] hybridized carbon materials in the ICPs compound. This peak has the highest density when the ICP concentration is increased to 40% and is hardly visible for the filament with 10% ICP content.

Energy-dispersive X-ray spectroscopy (EDS) confirmed the presence of ICP in the core of the filament, Fig 2 (c,d,e). EDS line scanning, the blue arrow in Fig 2(b), and the graph in Fig 2(c) show a small amount of ICP and high carbon content toward the outer part of the filament (shell). At the same time, intense iodine signals are present toward the middle part (core), suggesting a core/shell structure with good encapsulation of ICP inside the PCL shell. It should also be noted that some of the ICP compounds were infused into the PCL shell during the spinning process, which was confirmed with XPS data, Fig 3(f), referring to the spectra with a high-resolution scan of ICP iodine I 3d doublet is detected at ~619 eV ($I3d_{5/2}$) and ~632 eV ($I3d_{3/2}$) in the as-fabricated 30I-PCL and 40I-PCL samples. After degradation, it is evident that iodine is not detected in any sample, as the ICP in the shell part defused to the media quickly and caused the burst release of ICP to the media as confirmed by ICP concentration in media after 1 and 2 days, Fig 3(d).

To evaluate the stability and release rate of ICP into the media before complete suture degradation, the contrast property and release rate was measured in PBS at 37 °C with mild shaking for 22 days. The iodine concentration (from the ICPs) in the media was quantified by Inductively Coupled Plasma Mass Spectrometry (ICP-MS), Fig 3(d) and UV–Vis spectroscopy). There is a burst release of ICP after 24 hrs from all the sutures with various ICP concentrations due to the open end of the suture in media (the end of the suture was not sealed), which leads to the initial release of ICP at a high rate. This burst release could also be related to the possible presence of free iodine ions on the materials during the fabrication due to the reaction between iodoacetic acid and cysteine, Fig. 1S(b) (Supporting Information). This burst release can prevent the colonization of wounds with pathogenic microorganisms. However, after 48 hrs, there was a significant drop in ICP concentration in the media, which maintained steady till day 22. For example, the ICP concentration for 40I-PCL suture is 1739 ppb after 24 hrs, 199 ppb on day 2 and 145 ppb on day 22.

The degraded sutures composition was also analysed using FTIR spectroscopy, Fig 2S(b). After 22 days in media, the presence of ICP composite in the suture was confirmed by the C = C stretching vibration peak of ICP at 1601 cm^{-1} peak, especially for the suture with a 40% ICP concentration. However, this peak is smaller than the virgin suture due to the release of ICP into the media over 22 d

Contrast enhancement of I-PCL suture in medical image modalities. The effects of ICP concentration on contrast properties of I-PCL sutures were investigated by micro-CT imaging. To evaluate the detection limit of I-PCL by CT images. We compared micro-CT images (Hounsfield unit, HU) of sutures with various ICP concentrations. Water was used as the calibrating material with 0 HU as the recognized standard to calibrate the contrast effect of the I-PCL suture. The density of a sample (I-PCL suture here) is represented using the Hounsfield scale, with water having a value of zero Hounsfield units (HU) and samples denser than water having positive and samples less dense than water having negative values. The I-PCL suture's contrast effect increases with increasing ICP concentration in PCL and was distinguished by micro-CT images, Fig. 3(a,k). The contrast enhancement of 40I-PCL is 504.6 HU, which is 272%, 81%, and 31% higher than the I-PCL suture with 10, 20 and 30% ICP concentrations, respectively. Therefore, the 40I-PCL suture was

selected for further CT imaging study as it has the highest contrast enhancement.

To understand the effect of the PCL shell on the reduction of the contrast property of the ICP, the CT contrast property of 40ICP (core only) was recorded and calculated from the HU number. The 40ICP (core only) contrast enhancement was 699 HU% [1], 27% higher than the 40I-PCL core/shell suture.

The contrast property of the 40I-PCl was recorded after placing it in PBS for 22 days to investigate the effect of degradation on the contrast property of the suture and the release rate of ICP. The contrast enhancement of 40I-PCL was dropped by 18% after 22 days in PBS at 37 °C, which is still acceptable and is expected for the degradable suture. However, this amount is lower than the 40ICP due to the PCL shell barrier used for 40I-PCL, which decreases the ICP release into the media.

Due to the highest contrast enhancement, the 40I-PCL suture was selected to assess the possibility of suture application inside the tissue system. The selected suture was placed inside the chicken breast and thigh. The tissue was evaluated by micro-CT imaging. The C.T. images revealed that the 40I-PCL sutures in the chicken breast and thigh are clearly visible and distinguished from the tissue. Such visibility is anticipated to be advantageous for wound monitoring post-surgery, ultimately benefiting patient outcomes. Specifically, the use of material with these visible properties will improve the ability to identify the wound's location and monitor the healing process.

3.2. Antibacterial properties

Although the closure of clean surgical wounds can be accomplished using a wide variety of suture materials, the closure of contaminated wounds (i.e., those with an infected total joint arthroplasty) magnifies the properties of the individual suture types and their association with a bacterial infection [4,21,22]. *Staphylococcus aureus* with methicillin resistance is the most prevalent cause of surgical site infections [2,7,23]. Therefore, methicillin-resistant *S. aureus* (MRSA) was selected to study its interaction with I-PCL suture with various ICP concentrations. Bacterial viability and biofilm development on the 0,10,20,30 and 40I-PCL were also investigated. Fig. 4 shows that the increasing level of ICP resulted in inhibiting MRSA survival, adhesion, and biofilm formation. 30I-PCL

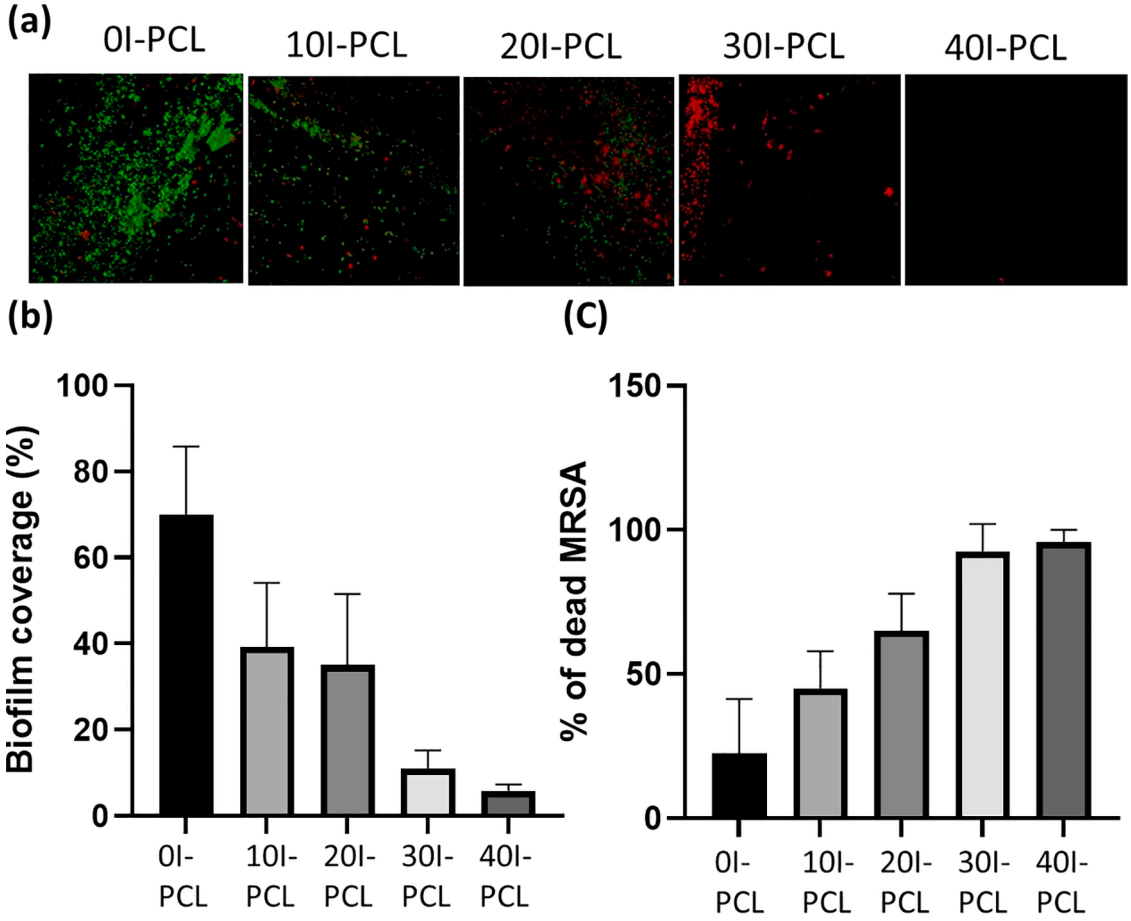

Fig. 4. Antibacterial performance of ICP embedded PCL sutures (I-PCL) against methicillin-resistant *Staphylococcus aureus* (MRSA). (a) CLSM images (green: viable; red: dead cells) show MRSA colonization on I-PCL sutures (scale bar = 20 μm). (b) The graph shows the biofilm coverage of MRSA over I-PCL sutures after 6 h incubation at 37°C. (c) The graph showing the percentage of dead MRSA on the I-PCL sutures.

was found to kill 90% of MRSA, and by increasing the ICP concentration in the suture to 40% (40I-PCL), MRSA was eliminated by nearly 99%, with no visible biofilm on the suture. These antimicrobial properties likely occur due to the ability of ICP, as a nanoparticle, to quickly enter bacteria and oxidize essential proteins, nucleotides, and fatty acids, ultimately leading to cell death [16,17].

3.3. *In-vitro cytotoxicity of I-PCL sutures*

Biocompatibility was assessed by culturing L929 mouse fibroblasts on 5 mg of each filament type: 0, 10, 20, 30 and 40I-PCL over a 48 h exposure period. The control was 0I-PCL, and a substrate of biocompatible silicone glue was also used to adhere 5 mg of each suture to the bottom of the cell culture plates. Cell viability was determined via two methods (following ISO 10993–5) -(1) a resazurin assay with fluorescence reading and (2) fluorescent staining of the cells and examination via confocal laser scanning microscopy (CLSM) to determine cell proliferation and attachment sites. The resazurin staining assay determines the amount of metabolically active cells as resazurin is reduced by live cells to resorufin, a highly fluorescent compound. The resazurin staining assay, Fig. 5(a), shows that the 0, 10, and 20I-PCL sutures have a negligible effect on cell viability after 48 h. However, the 30 and 40I-PCL sutures showed moderate cytotoxicity. These sutures showed some cell growth inhibition, with the 30I-PCL having 61.24% viability and the 40I-PCL having 54.47% viability compared with the silicone control. This is likely due to the high ICP concentrations in the suture and its release to the media (burst release of ICP over 48 hrs, Fig 23(d)), as reflected in the 10I-PCL (89.03%) and 20I-PCL (93.22%) sutures that have lower cell viability than the 0I-PCL suture (control, 96.22%).

For the CLSM images, Fig 5(b-f), the nuclei of the L929 mouse fibroblasts were stained with DAPI and actin filaments were stained with rhodamine-phalloidin. CLSM images confirmed that cells were able to adhere to all sutures. However, the quantitative assessment of cell growth on each type of suture was challenging due to the 3-dimensional nature of the samples and the inhomogeneous distribution of cells on the filaments. In addition, viable cells were also found on the silicon glue used to fix the I-PCL sutures to the bottom of the cell culture plate (Fig. 4g).

In summary, developing sutures that can be visualized under the image modalities such as CT and MRI imaging can minimize the risks mentioned above, support monitoring internal wounds and assist surgeons in being able to accurately plan surgery if mesh complications develop requiring mesh removal [24,25]. Furthermore, given the unique properties of heteroatom carbon nanoparticles, including fluorescence, contrasting image effects and antibacterial properties, biocompatible carbon dot filaments have the potential to replace the current conventional suture used in the current surgical procedure [12,14,15,26,27]. In this context, 40I-PCL is a representative material that satisfies various requirements for medical applications by providing imaging capabilities, moderate biocompatibility and excellent antimicrobial properties.

The slow release of ICPs from the suture to the surrounding milieu provides good biocompatibility and antibacterial properties and prevents biofilm formation, as demonstrated in cell culture media. Additionally, ICP sutures can be visualized during and after surgery by including only a small amount (<1%) of ICP in the suture that remains in the targeted area and is slowly released over an extended time. Typical doses for CT scans provide 2500 to 5000 μg of bioavailable free iodine and 15 to 37 g of total iodine [28]; however, in this study, the maximum concentration of iodine in the media is approximately 150 to 180 μg (1.5–1.8 ppm), Fig. 3(d), which can be considered safe relevant to currently accepted procedures [18,28].

This contrast suture (I-PCL) has properties such as a longer life (staying longer in the media) with less toxicity than a traditional intravenous contrast agent, which results in broader, safer, and more accessible medical applications. The optimal concentration of ICP in the I-PCL filament is 40%, as demonstrated by its clear visibility under CT imaging both before and after degradation, along with the highest antimicrobial activities and lowest biofilm formation, which are due to the presence of sufficient ICP both on and off adjacent to the suture surface. 10I-PCL and 20I-PCL sutures were deemed biocompatible following ISO 10993–5 cell viability experiment

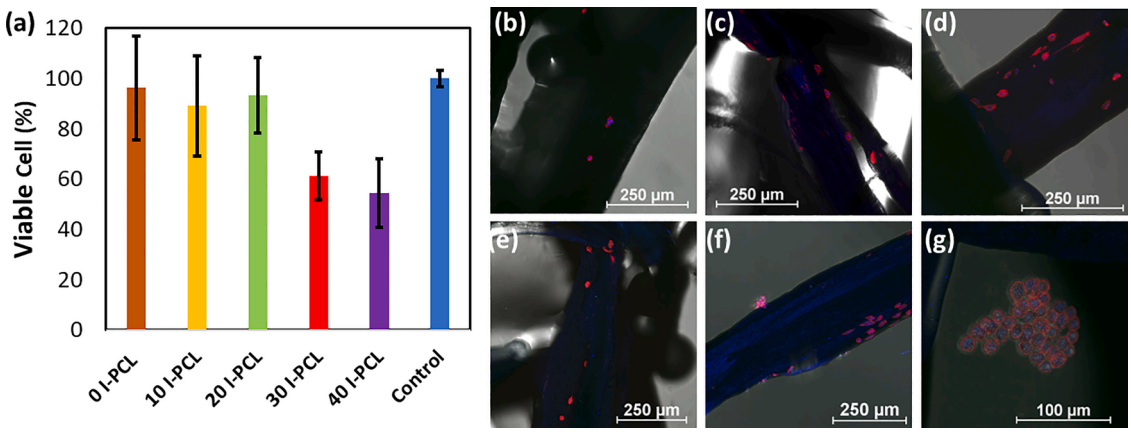

Fig. 5. Cell viability of L929 fibroblasts after 48 h incubation on I-PCL sutures and control. CLSM images of the fibroblasts, stained with DAPI and rhodamine-phalloidin. (a) Cell viability incubated on I-PCL sutures and control as quantified by a resazurin assay. (b) 0I-PCL, (c) 10I-PCL, (d) 20I-PCL, (e) 30I-PCL, (f) 40I-PCL, and (g) cluster of cells grown on silicone glue, which was used to fix the sutures to the bottom of the tissue culture plate.

protocols; however, 30I-PCL and 40I-PCL sutures showed moderate cytotoxicity (as defined by ISO 10933–5), which could be due to the high release of ICP into the media in the first 48 h. In summary, the 40I-PCL suture has the best visibility, moderate biocompatibility, and slow ICP release, contributing to the best antimicrobial activities that facilitate biofilm formation and wound infection, enabling non-invasive post-surgical monitoring.

4. Conclusion

This research designed a multifunctional and biocompatible I-PCL suture composed of a radiopaque ICP core with an inherent imaging capability and a biocompatible PCL shell. This suture provides good mechanical properties and flexibility, suitable for suture applications while being clearly visualized under imaging modalities, including CT scan imaging. The visualization can monitor the wound site, suture degradation and disappearance after the surgery. In addition, the developed suture possesses enhanced antimicrobial properties combined with low or suppressed toxicity due to the presence and release of ICP over an extended time. This slow-release property assists in the prevention of biofilm formation and infection of the suture after the surgery. This research provides additional insights into the possible application of multifunctional core-shell sutures with enhanced antimicrobial properties and viability for increased post-surgery monitoring and infection control.

CRediT authorship contribution statement

Shadi Houshyar: Conceptualization, Methodology, Validation, Investigation, Formal analysis, Writing – original draft, Supervision. **Hong Yin:** Methodology, Validation, Formal analysis, Writing – original draft, Writing – review & editing. **Leon Pope:** Methodology, Validation, Formal analysis, Writing – original draft, Writing – review & editing. **Rumbidzai Zizhou:** Validation, Investigation, Writing – review & editing. **Chaitali Dekiwadia:** Methodology, Formal analysis, Writing – review & editing. **Elisa L. Hill-Yardin:** Conceptualization, Supervision, Writing – review & editing. **Justin MC Yeung:** Supervision, Writing – review & editing. **Sabu John:** Writing – review & editing. **Kate Fox:** Supervision, Resources, Formal analysis, Writing – review & editing. **Nhiem Tran:** Supervision, Formal analysis, Writing – review & editing. **Ivan Cole:** Supervision, Resources, Writing – review & editing. **Aaron Elbourne:** Methodology, Validation, Writing – review & editing. **Vi Khanh Truong:** Methodology, Validation, Formal analysis, Writing – original draft, Writing – review & editing. **Adam Truskewycz:** Conceptualization, Methodology, Validation, Writing – review & editing.

Declaration of Competing Interest

The authors declare no competing financial interest.

Acknowledgments

The authors acknowledge the support from the scientific and technical assistance of the RMIT University Microscopy and Microanalysis Facility, a linked laboratory of Microscopy Australia. In addition, S.H. acknowledges the support of an RMIT Vice-Chancellor Fellowship.

Supplementary materials

Supplementary material associated with this article can be found, in the online version, at doi:10.1016/j.onano.2022.100120.

References

[1] Maida Šiširak*, A. Z, Mirsada Hukić, Methicillin-resistant staphylococcus aureus (MRSA) as a cause of nosocomial wound infections, Bosn. J. Basic Med. Sci. 10 (1) (2010) 32–37.
[2] R.J. Gordon, F.D. Lowy, Pathogenesis of Methicillin-Resistant Staphylococcus aureus Infection, Clin. Infect. Dis. 46 (Supplement_5) (2008) S350–S359.
[3] C.D. Owens, S. K, Surgical site infections: epidemiology, microbiology and prevention, J. Hosp. Infect. 70 (S2) (2008) 3–10.
[4] S. Kathju, L. Nistico, L. Hall-Stoodley, J.C. Post, G.D. Ehrlich, P. Stoodley, Chronic surgical site infection due to suture-associated polymicrobial biofilm, Surg. Infect. (Larchmt) 10 (5) (2009) 457–461.
[5] F. Wu, C. Tan, Dead bacterial absorption of antimicrobial peptides underlies collective tolerance, J. R. Soc. Interface 16 (151) (2019), 20180701.
[6] A.L. Gallo, F. Paladini, A. Romano, T. Verri, A. Quattrini, A. Sannino, M. Pollini, Efficacy of silver coated surgical sutures on bacterial contamination, cellular response and wound healing, Mater. Sci. Eng. C Mater. Biol. Appl. 69 (2016) 884–893.
[7] A.M. Elward, J.M. McAndrews, V.L. Young, Methicillin-sensitive and methicillin-resistant staphylococcus aureus: preventing surgical site infections following plastic surgery, Aesthet. Surg. J. 29 (3) (2009) 232–244.
[8] D.H. Ballard, U. Jammalamadaka, K. Tappa, J.A. Weisman, C.J. Boyer, J.S. Alexander, P.K. Woodard, 3D printing of surgical hernia meshes impregnated with contrast agents: in vitro proof of concept with imaging characteristics on computed tomography, 3D Print Med. 4 (1) (2018) 13.
[9] M.V. Spampinato, A. A, M.G. Matheus, Current Radiographic Iodinated Contrast Agents, Magn. Reson. Imaging Clin. N. Am. 25 (4) (2017) 697–704.
[10] A. Baek, H.-k. Kim, J.-u. Yang, G. Choi, M. Kim, A.E. Cho, Y.-h. Kim, S. Kim, B. Sung, B. Woo Yang, H. Seo, G.-.H. Lee, H.-.K. Ryeom, H. Jung, T. Lee, Y. Chang, High-performance hepatobiliary dysprosium contrast agent for ultra-high-field magnetic resonance imaging, J. Ind. Eng. Chem. 85 (2020) 297–307.
[11] E.S. Rowe, V.D. Rowe, S. Biswas, G. Mosher, L. Insisienmay, M.K. Ozias, M.R. Gralinski, J. Hunter, J.S. Barnett, Preclinical Studies of a Kidney Safe Iodinated Contrast Agent, J. Neuroimaging 26 (5) (2016) 511–518.

[12] K. Shin, J.W. Choi, G. Ko, S. Baik, D. Kim, O.K. Park, K. Lee, H.R. Cho, S.I. Han, S.H. Lee, D.J. Lee, N. Lee, H.C. Kim, T. Hyeon, Multifunctional nanoparticles as a tissue adhesive and an injectable marker for image-guided procedures, Nat. Commun. 8 (2017) 15807.
[13] K.R. Sneha, P.S. Steny, G.S. Sailaja, Intrinsically radiopaque and antimicrobial cellulose based surgical sutures from mechanically powerful Agave sisalana plant leaf fibers, Biomater. Sci. 9 (23) (2021) 7944–7961.
[14] F. Yuan, T. Yuan, L. Sui, Z. Wang, Z. Xi, Y. Li, X. Li, L. Fan, Z. Tan, A. Chen, M. Jin, S. Yang, Engineering triangular carbon quantum dots with unprecedented narrow bandwidth emission for multicolored LEDs, Nat. Commun. 9 (1) (2018) 2249.
[15] H. Aviv, S. Bartling, F. Kieslling, S. Margel, Radiopaque iodinated copolymeric nanoparticles for X-ray imaging applications, Biomaterials 30 (29) (2009) 5610–5616.
[16] D. Lepelletier, J.Y. Maillard, B. Pozzetto, A. Simon, Povidone Iodine: properties, Mechanisms of Action, and Role in Infection Control and Staphylococcus aureus Decolonization, Antimicrob. Agents Chemother. 64 (9) (2020) e00682-20.
[17] X. Li, B. Wang, T. Liang, R. Wang, P. Song, Y. He, Synthesis of cationic acrylate copolyvidone-iodine nanoparticles with double active centers and their antibacterial application, Nanoscale 12 (42) (2020) 21940–21950.
[18] Kaller, M.O.; An, J., Contrast Agent Toxicity. BTI - StatPearls.
[19] N. Ikeda, S. Fujibayashi, S. Yamaguchi, K. Goto, B. Otsuki, T. Kawai, T. Shimizu, Y. Okuzu, K. Masamoto, Y. Shimizu, Y. Takaoka, S. Matsuda, Bioactivity and antibacterial activity of iodine-containing calcium titanate against implant-associated infection, Biomater. Adv. 138 (2022), 212952.
[20] C. Freeman, E. Duan, J. Kessler, Molecular iodine is not responsible for cytotoxicity in iodophors, J. Hosp. Infect. 122 (2022) 194–202.
[21] S. Morrison, A. Singh, J. Rousseau, J.S. Weese, Adherence of methicillin-resistant Staphylococcus pseudintermedius to suture materials commonly used in small animal surgery, Am. J. Vet. Res. 77 (2) (2016) 194–198.
[22] A. Clinton, T. Carter, Chronic wound biofilms: pathogenesis and potential therapies, Lab. Med. 46 (4) (2015) 277–284.
[23] Hoffmann, J.P.; Friedman, J.K.; Wang, Y.; McLachlan, J.B.; Sammarco, M.C.; Morici, L.A.; Roy, C.J., In situ treatment with novel microbiocide inhibits methicillin resistant Staphylococcus aureus in a murine wound infection model. 2020, 10 (3106).
[24] Y. Ju, B. Dong, J. Yu, Y. Hou, Inherent multifunctional inorganic nanomaterials for imaging-guided cancer therapy, Nano Today 26 (2019) 108–122.
[25] S.R. Jernigan, G. Chanoit, A. Veeramani, S.B. Owen, M. Hilliard, D. Cormier, B. Laffitte, G. Buckner, A laparoscopic knot-tying device for minimally invasive cardiac surgery, Eur. J. Cardiothorac. Surg. 37 (3) (2010) 626–630.
[26] M. Omidi, A. Yadegari, L. Tayebi, Wound dressing application of pH-sensitive carbon dots/chitosan hydrogel, RSC Adv. 7 (18) (2017) 10638–10649.
[27] P. Yang, Z. Zhu, T. Zhang, W. Zhang, W. Chen, Y. Cao, M. Chen, X. Zhou, Orange-emissive carbon quantum dots: toward application in wound pH monitoring based on colorimetric and fluorescent changing, Small 15 (44) (2019), e1902823.
[28] S.Y. Lee, C.M. Rhee, A.M. Leung, L.E. Braverman, G.A. Brent, E.N. Pearce, A review: radiographic iodinated contrast media-induced thyroid dysfunction, J. Clin. Endocrinol. Metab. 100 (2) (2015) 376–383.